



A novel N-hydroxy-N'-aminoguanidine derivative inhibits ribonucleotide reductase activity: Effects in human HL-60 promyelocytic leukemia cells and synergism with arabinofuranosylcytosine (Ara-C)

Philipp Saiko^a, Geraldine Graser^a, Benedikt Giessrigl^b, Andreas Lackner^c, Michael Grusch^c, Georg Krupitza^b, Arijit Basu^d, Barij Nayan Sinha^d, Venkatesan Jayaprakash^d, Walter Jaeger^e, Monika Fritzer-Szekeres^a, Thomas Szekeres^{a,*}

^a Department of Medical and Chemical Laboratory Diagnostics, Medical University of Vienna, General Hospital of Vienna, Waehringer Guertel 18-20, A-1090 Vienna, Austria

^b Institute of Clinical Pathology, Medical University of Vienna, Waehringer Guertel 18-20, A-1090 Vienna, Austria

^c Department of Medicine I, Division of Cancer Research, Medical University of Vienna, Borschkegasse 8a, A-1090 Vienna, Austria

^d Department of Pharmaceutical Sciences, Birla Institute of Technology, Mesra 835 215, India

^e Department of Clinical Pharmacy and Diagnostics, Faculty of Life Sciences, University of Vienna, Althanstrasse 14, A-1090 Vienna, Austria

ARTICLE INFO

Article history:

Received 13 July 2010

Accepted 7 September 2010

Keywords:

N-hydroxy-N'-aminoguanidines

Ribonucleotide reductase

Cell cycle arrest

Arabinofuranosylcytosine

Synergistic combination effects

ABSTRACT

Ribonucleotide reductase (RR; EC 1.17.4.1) is responsible for the *de novo* conversion of ribonucleoside diphosphates into deoxyribonucleoside diphosphates, which are essential for DNA replication. RR is upregulated in tumor cells and therefore considered to be an excellent target for cancer chemotherapy.

ABNM-13 (N-hydroxy-2-(anthracene-2-yl-methylene)-hydrazinecarboximidamide), a novel N-hydroxy-N'-aminoguanidine has been designed to inhibit RR activity using 3D molecular space modeling techniques. In this study, we evaluated its effect on human HL-60 promyelocytic leukemia cells. ABNM-13 proved to be a potent inhibitor of RR which was displayed by significant alterations of deoxyribonucleoside triphosphate (dNTP) pool balance and a highly significant decrease of incorporation of radiolabeled cytidine into DNA of HL-60 cells. Diminished RR activity caused replication stress which was consistent with activation of Chk1 and Chk2, resulting in downregulation/degradation of Cdc25A. In contrast, Cdc25B was upregulated, leading to dephosphorylation and activation of Cdk1. The combined dysregulation of Cdc25A and Cdc25B was the most likely cause for ABNM-13 induced S-phase arrest. Finally, we combined ABNM-13 with the first-line antileukemic agent arabinofuranosylcytosine (Ara-C) and found that ABNM-13 synergistically potentiated the antineoplastic effects of Ara-C.

Due to these promising results, ABNM-13 deserves further preclinical and *in vivo* testing.

© 2010 Elsevier Inc. All rights reserved.

1. Introduction

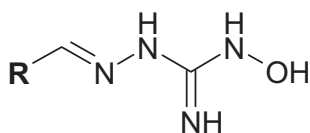
Various compounds with hydroxyguanidine, thiosemicarbazide, and substituted benzohydroxamic acid functional groups have shown promising antitumor activity [1–5]. Hydroxyguanidines and hydroxysemicarbazides were especially active against human CCRF-CEM/O and murine L1210 leukemia cells as well as against human HT-29 colon cancer cells [1–4,6]. These agents inhibited DNA synthesis as a consequence of inhibiting ribonucleotide reductase (RR; EC 1.17.4.1) activity.

RR is significantly upregulated in tumor cells in order to meet the increased need for deoxyribonucleoside triphosphates (dNTPs) of these rapidly proliferating cells for DNA synthesis [7]. The

enzyme is an $\alpha 2 \beta 2$ complex consisting of two subunits [8]. The effector binding R1 subunit possesses an $\alpha 2$ homodimeric structure with substrate and allosteric effective sites that control enzyme activity and substrate specificity. The nonheme iron R2 subunit, a $\beta 2$ homodimer, forms two dinuclear iron centers each stabilizing a tyrosyl radical. The inhibition of the nonheme iron subunit can be caused, for instance, by iron chelation or radical scavenging of the tyrosyl radical [9]. Additionally, a p53-inducible R2-homologue (p53R2) has been described recently [9]. Expression of the R2 and p53R2 subunits is induced by DNA damage and it has been reported that p53R2 supplies dNTPs for DNA repair in G₀/G₁ cells in a p53-dependent manner [10]. Hydroxyurea (HU) is the first RR inhibitor that has been used in clinical practice and is given to treat chronic myeloid leukemia and many other neoplastic diseases [11,12]. Difluorodeoxycytidine (Gemcitabine; dFdC) is applied in chemotherapy regimens against non-small cell lung cancer and pancreatic cancer [13,14].

* Corresponding author. Tel.: +43 1 40400 5365; fax: +43 1 320 33 17.
E-mail address: thomas.szekeres@meduniwien.ac.at (T. Szekeres).

HU is believed to destabilize R2 iron centers by scavenging the tyrosyl radical which is essential for enzyme activity [9,15]. Several newer iron chelating agents including tachypyridine [16–20] and a



ABNM	R	IC ₅₀ (μM)
1		> 100
2		> 100
3		> 100
4		95
5		> 100
6		> 100
7		> 100
8		67
9		60
10		> 100
11		> 100
12		62
13		11

Fig. 1. Structural formula and biological activity of ABNM 1–13 in HL-60 cells. HL-60 cells (0.1×10^6 per ml) were incubated with increasing concentrations of drugs for 72 h. Cell counts and IC₅₀ values (IC₅₀ = 50% growth inhibition of tumor cells) were determined using a microcellcounter CC-110. Viability of cells was determined by trypan blue staining. Results were calculated as number of viable cells. Data are means \pm standard errors of three determinations.

number of thiosemicarbazones such as triapine [9,21] were shown to interact with the iron-containing R2 subunit. These compounds are currently under (pre)clinical development.

Modern drug design uses qualitative and quantitative structure–activity relationship (QSAR) studies as an approach to find relationships between chemical structures or structure-related properties and biological activities of distinct compounds. Based on the prediction of the best QSAR model, we synthesized 13 novel compounds (ABNM-1 to ABNM-13) with potential RR inhibitory capacities. Five of these agents were active in human HL-60 promyelocytic leukemia cells and ABNM-13 was chosen as lead substance because of its pronounced growth inhibitory effects which were up to 10-fold stronger than those of HU. The HL-60 cell line is an excellent *in vitro* model and has been extensively used by our group and others, especially with regard to investigate RR activity after treatment with various drugs. Additionally, growth inhibition and cytotoxicity caused by ABNM-13 were also investigated in human AsPC-1 pancreatic cancer cells. To study the mechanisms by which ABNM-13 influences cell cycle transit in HL-60 cells, we examined the effects on RR and the cell cycle regulators downstream of checkpoint kinase activation.

In general, anticancer drugs are more effective when used in combination. The major advantage of drug combinations is the achievement of additive or synergistic effects through intimidation of distinct molecular pathways and, accordingly, a decrease of drug resistance. For example, administration of leucovorin increases the binding of an active 5-fluorouracil metabolite to its target, thymidylate synthase, thus increasing the antineoplastic effects [22]. In addition, various RR inhibitors caused synergism together with arabinofuranosylctosine (Ara-C), a first line antileukemia drug affecting intracellular dCTP pools [23–27]. Following this strategy, we combined ABNM-13 with Ara-C in order to test potential additive or synergistic properties.

2. Materials and methods

2.1. Chemicals and supplies

ABNM 1–13 were synthesized and provided by the Department of Pharmaceutical Sciences, Birla Institute of Technology, Mesra, India. Structural formulas are shown in Fig. 1. Ara-C, HU and all other chemicals and reagents were commercially available (Sigma–Aldrich, Vienna, Austria) and of highest purity.

2.2. Cell culture

The human HL-60 promyelocytic leukemia and human AsPC-1 pancreatic adenocarcinoma cell lines were purchased from ATCC (American Type Culture Collection, Manassas, VA, USA). Both lines were grown in RPMI 1640 medium supplemented with 10% heat inactivated fetal calf serum (FCS), 1% L-glutamine, and 1% penicillin–streptomycin at 37 °C in a humidified atmosphere containing 5% CO₂ using a Heraeus cytoperm 2 incubator (Heraeus, Vienna, Austria). AsPC-1 cells were grown in a monolayer culture using 25 cm² tissue culture flasks and were periodically detached from the flask surface by 0.25% trypsin–ethylenediaminetetraacetic acid (trypsin–EDTA) solution. All media and supplements were obtained from Life Technologies (Paisley, Scotland, UK). Cell counts were determined using a microcellcounter CC-110 (SYS-MEX, Kobe, Japan). Cells growing in the logarithmic phase of growth were used for all experiments described below.

2.3. Growth inhibition assay

HL-60 cells (0.1×10^6 per ml) were seeded in 25 cm² Nunc tissue culture flasks and incubated with increasing concentrations

of ABNM-13 or HU at 37 °C under cell culture conditions. Cell counts and IC₅₀ values (IC₅₀ = 50% growth inhibition of tumor cells) were determined after 24, 48, and 72 h using a microcellcounter CC-110.

In another set of experiments, AsPC-1 cells were seeded in 25 cm² Nunc tissue culture flasks and allowed to attach overnight. Cells were then incubated with increasing concentrations of ABNM-13 for 72 h. After that period, cells were detached from the flask surface by 0.25% trypsin–ethylenediaminetetraacetic acid (trypsin–EDTA) solution. After removal of trypsin–EDTA by centrifugation and suspension of the pellet in RPMI 1640 medium, cells were counted using a microcellcounter CC-110. Viability of cells was determined by staining with trypan blue. Results were calculated as number of viable cells.

2.4. Clonogenic assay

AsPC-1 cells (2×10^3 per well) were plated in 24-well plates and allowed to attach overnight at 37 °C in a humidified atmosphere containing 5% CO₂. Then cells were incubated with increasing concentrations of ABNM-13 for 6 days. Subsequently, the medium was carefully removed from the wells and the plates were stained with 0.5% crystal violet solution for 5 min. Colonies of more than 50 cells were counted using an inverted microscope at 40-fold magnification.

2.5. MTT chemosensitivity assay

AsPC-1 or HL-60 cells (5×10^3 per well) were seeded in 96-well microtiter plates in supplemented RPMI 1640 medium. AsPC-1 cells were allowed to attach overnight. Cells were then incubated with various concentrations of ABNM-13 for 96 h at 37 °C under cell culture conditions. After that period, the reduction of the yellow tetrazolium compound 3-(4,5-dimethylthiazo-2-yl)-2,5-diphenyl tetrazoliumbromide (MTT) by the mitochondrial dehydrogenases of viable cells to a purple formazan product was determined using an assay kit from Promega® according to the supplier's manual. The change in absorbance at 550 nm was tracked on a Wallac 1420 Victor 2 multilabel plate reader (PerkinElmer Life and Analytical Sciences). Drug effect was quantified as the percentage of control absorbance of reduced dye at this wavelength.

2.6. Simultaneous growth inhibition assay using ABNM-13 and Ara-C

HL-60 cells (0.1×10^6 per ml) were simultaneously incubated with various concentrations of ABNM-13 (12.5, 15, 17.5, and 20 μM) and Ara-C (10, 15, and 20 nM) for 72 h. After that period, cells were counted using a microcellcounter CC-110.

2.7. Sequential growth inhibition assay using ABNM-13 and Ara-C

HL-60 cells (0.1×10^6 per ml) were first incubated with different concentrations of ABNM-13 (2.5, 5, 7.5, and 10 μM) for 24 h. Then ABNM-13 was washed out and cells were further exposed to various concentrations of Ara-C (10, 15, and 20 nM) for another 48 h. After that period, cells were counted using a microcellcounter CC-110.

2.8. Cell cycle distribution analysis

Cells (0.4×10^6 per ml) were seeded in 25 cm² Nunc tissue culture flasks and incubated with increasing concentrations of drugs at 37 °C under cell culture conditions. After 24 h, cells were harvested and suspended in 5 ml cold PBS, centrifuged, resuspended and fixed in 3 ml cold ethanol (70%) for 30 min at 4 °C. After

two washing steps in cold PBS RNase A and propidium iodide were added to a final concentration of 50 μg/ml each and incubated at 4 °C for 60 min before measurement. Cells were analyzed on a FACSCalibur flow cytometer (BD Biosciences, San Jose, CA, USA) and cell cycle distribution was calculated with ModFit LT software (Verity Software House, Topsham, ME, USA).

2.9. Western blotting

After incubation with 15 μM ABNM-13 and/or 15 nM Ara-C, HL-60 cells (2×10^6 per ml) were harvested, washed twice with ice-cold PBS (pH 7.2) and lysed in a buffer containing 150 mM NaCl, 50 mM Tris-buffered saline (Tris pH 8.0), 1% Triton X-100, 2.5% 100 mM phenylmethylsulfonylfluoride (PMSF) and 2.5% protease inhibitor cocktail (PIC; from a 100× stock). The lysate was centrifuged at 12,000 rpm for 20 min at 4 °C, and the supernatant was stored at –20 °C until further analysis. Equal amounts of protein samples were separated by polyacrylamide gel electrophoresis (PAGE) and electroblotted onto PVDF membranes (Hybond, Amersham) overnight at 4 °C. Equal sample loading was controlled by staining membranes with Ponceau S. After washing with PBS/Tween-20 (PBS/T) pH 7.2 or Tris/Tween-20 (TBS/T) pH 7.6, membranes were blocked for 60 min in blocking solution (5% non-fat dry milk in PBS containing 0.5% Tween-20 or in TBS containing 0.1% Tween-20). Then membranes were incubated with the first antibody (in blocking solution, dilution 1:500 to 1:1000) by gently rocking at 4 °C, overnight. Subsequently, the membranes were washed with PBS or TBS and further incubated with the second antibody (peroxidase-conjugated goat anti-rabbit IgG, anti-mouse IgG, or donkey anti-goat IgG – dilution 1:2000 to 1:5000 in PBS/T or TBS/T) at room temperature for 60 min. Chemiluminescence was developed by the ECL detection kit (Amersham, Buckinghamshire, UK) and then membranes were exposed to Amersham Hyperfilms.

Equal numbers of cells were lysed for each sample, protein content was measured by the Bradford method, and PVDF membranes were checked by Ponceau S staining. Equal sample loading was controlled by β-actin expression which appeared to be stable when inspected in short term exposures to X-ray films. Each Western blot experiment was performed at least twice, and specific experimental points were done more often as they served as internal controls.

Antibodies directed against p(Ser1981)-ATM, p(Ser317)-Chk1, Chk1, p(Thr68)-Chk2, Chk2, p(Tyr15)-Cdc2, cleaved Caspase-3 (Asp175) and anti-rabbit IgG were from Cell Signaling (Danvers, MA, USA), against p(Ser75)-Cdc25A from Abcam (Cambridge, MA, USA), against p(Ser177)-Cdc25A from Abgent (San Diego, CA, USA), against R1 (T-16), R2 (I-15), p53R2 (N-16), Cdc25A (F-6), Cdc25B (C-20), Cdc25C (C-20), Cdc2 p34 (17), and donkey anti-goat IgG from Santa Cruz (Santa Cruz, CA, USA), against ph(Ser139)-γH2AX from Merck (Darmstadt, Germany), against β-actin from Sigma (St. Louis, MO, USA), and anti-mouse IgG was from Dako (Glostrup, Denmark).

2.10. Incorporation of ¹⁴C-labeled cytidine into DNA (DNA synthesis assay)

To analyze the effect of ABNM-13 treatment on the activity of DNA synthesis, an assay was performed as described previously [28]. Radiolabeled ¹⁴C-cytidine has to be reduced by RR in order to be incorporated into the DNA of HL-60 cells following incubation with ABNM-13 and/or Ara-C. HL-60 cells (0.4×10^6 cells per ml) were incubated with various concentrations of ABNM-13 for 24 h. After that, cells were counted and pulsed with ¹⁴C-cytidine (0.3125 μCi, 5 nM) for 30 min at 37 °C. In another set of experiments, cells were treated with ABNM-13 and/or Ara-C for 30 min and simultaneously pulsed with ¹⁴C-cytidine (0.3125 μCi,

5 nM). Afterwards, cells were collected by centrifugation and washed with PBS. Total DNA from 5×10^6 cells was purified by phenol–chloroform–isoamyl alcohol extraction and specific radioactivity of the samples was determined using a Wallac 1414 liquid scintillation counter (PerkinElmer, Boston, MA) whose read out was normalized by a Hitachi U-2000 Double Beam Spectrophotometer to ensure equal amounts and purity of DNA.

2.11. Determination of deoxyribonucleoside triphosphates (dNTPs)

Cells were seeded in 175 cm² tissue culture flasks (5×10^7 per flask) and incubated with increasing concentrations of ABNM-13 for 24 h. The cells were then centrifuged at $1800 \times g$ for 5 min, resuspended in 100 μ l of PBS, and extracted with 10 μ l of trichloroacetic acid (90%). The lysate was allowed to rest on ice for 30 min and neutralized by the addition of 1.5 volumes of freon containing 0.5 mol/l tri-n-octylamine. Concentrations of dNTPs were then determined using the method described by Garrett and Santi [29]. Aliquots (100 μ l) of the samples were analyzed using a Merck “La Chrom” high-performance liquid chromatography (HPLC) system (Merck, Darmstadt, Germany) equipped with D-7000 interface, L-7100 pump, L-7200 auto-sampler, and L-7400 UV detector. Detection time was set at 80 min, with the detector operating on 280 nm for 40 min and then switched to 260 nm for another 40 min. Samples were eluted with a 3.2 M ammonium phosphate buffer (pH 3.6, adjusted by the addition of 3.2 mM H₃PO₄) containing 20 M acetonitrile using a 4.6 \times 250 mm PARTISIL 10 SAX column (Whatman Ltd., Kent, UK). Separation was performed at constant ambient temperature and a flow rate of 2 ml per min. The concentration of each dNTP was calculated as percentage of the total area under the curve for each sample.

2.12. Hoechst dye 33258 and propidium iodide double staining

The Hoechst staining was performed according to the method described by our group [30]. HL-60 cells (0.2×10^6 per ml) were seeded in 25 cm² Nunc tissue culture flasks and exposed to increasing concentrations of ABNM-13 for 24 and 48 h. Hoechst 33258 (HO, Sigma, St. Louis, MO, USA) and propidium iodide (PI, Sigma, St. Louis, MO, USA) were added directly to the cells to final concentrations of 5 μ g/ml and 2 μ g/ml, respectively, followed by 60 min of incubation at 37 °C. Cells were examined on a Nikon Eclipse TE-300 Inverted Epi-Fluorescence Microscope (Nikon, Tokyo, Japan) equipped with a Nikon DS-5M-L1 Digital Sight Camera System including appropriate filters for Hoechst 33258 and PI. This method allows distinguishing between early apoptosis, late apoptosis, and necrosis and is therefore superior to TUNEL assay which fails to discriminate among apoptosis and necrosis [31,32] and does not provide any morphological information. In addition, the HO/PI staining is more sensitive than a customary FACS based Annexin V binding assay [32–34]. The Hoechst dye stains the nuclei of all cells and thus allows monitoring cellular changes associated with apoptosis, such as chromatin condensation and nuclear fragmentation. In contrast, PI is excluded from viable and early apoptotic cells; consequently, PI uptake indicates loss of membrane integrity being characteristic of late apoptotic and necrotic cells. In combination with fluorescence microscopy to evaluate the morphologies of nuclei, the selective uptake of the two dyes enables studying the induction of apoptosis in intact cultures and to distinguish it from non-apoptotic cell death by means of necrosis. The latter is characterized by nuclear PI uptake without chromatin condensation or nuclear fragmentation [35].

Cells were judged according to their morphology and the integrity of their cell membranes, counted under the microscope and the number of apoptotic cells was given as percentage value.

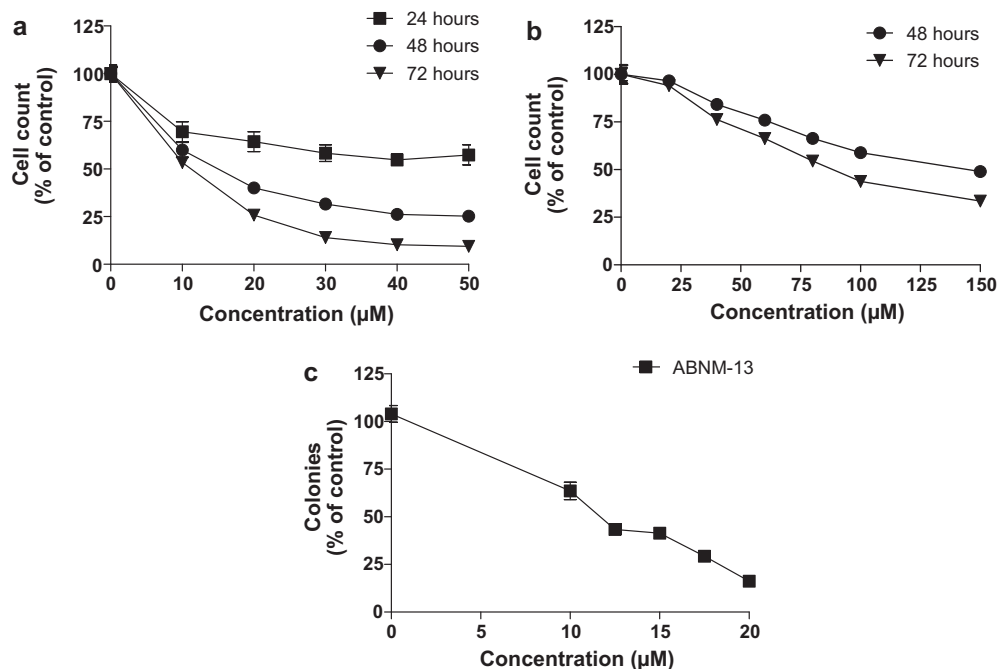


Fig. 2. (a and b) Growth inhibition of HL-60 cells after incubation with ABNM-13 or HU. HL-60 cells (0.1×10^6 per ml) were incubated with increasing concentrations of ABNM-13 or HU. Cell counts and IC₅₀ values (IC₅₀ = 50% growth inhibition of tumor cells) were determined using a microcellcounter CC-110. Viability of cells was determined by trypan blue staining. Results were calculated as number of viable cells. Data are means \pm standard errors of three determinations. (c) Inhibition of colony formation of AsPC-1 cells after incubation with ABNM-13. AsPC-1 cells (2×10^3 per well) were plated in 24-well plates and allowed to attach overnight at 37 °C in a humidified atmosphere containing 5% CO₂. After 24 h, the cells were incubated with increasing concentrations of ABNM-13 for 6 days. Subsequently, the medium was carefully removed from the wells and the plates were stained with 0.5% crystal violet solution for 5 min. Colonies of more than 50 cells were counted using an inverted microscope at 40-fold magnification. Data are means \pm standard errors of three determinations.

2.13. Statistical calculations

Dose–response curves were calculated using the Prism 5.01 software package (GraphPad, San Diego, CA, USA) and significant differences between controls and each drug concentration applied were determined by unpaired *t*-test. The calculations of dose–response curves and combination effects were performed using the “Calculusyn” software designed by Chou and Talalay (Biosoft, Ferguson, MO) [36]. The analytical method of Chou and Talalay [36,37] describes the interaction among drugs in a given combination. A combination index (CI) of <0.9 indicates synergism, a CI of 0.9–1.1 indicates additive effects, and a CI of >1.1 indicates antagonism.

3. Results

3.1. Effect of ABNM 1–13 on the growth of HL-60 and AsPC-1 cells

HL-60 cells (0.1×10^6 per ml) were seeded in 25 cm² Nunc tissue culture flasks and incubated with increasing concentrations of ABNM 1–13. After 72 h, the cell number of viable leukemia cells was determined. ABNM-4, ABNM-8, ABNM-9, ABNM-12, and ABNM-13 inhibited the growth of HL-60 cells with IC₅₀ values (IC₅₀ = 50% growth inhibition of tumor cells) of 95 ± 2.2 , 67 ± 1.3 , 60 ± 1.0 , 62 ± 2.0 , and 11 ± 1.1 μM, respectively. The IC₅₀ values of

all other compounds remained beyond 100 μM (Fig. 1). In another set of experiments, AsPC-1 cells (0.2×10^6 per ml) were seeded in 25 cm² Nunc tissue culture flasks and allowed to attach overnight. After 72 h, cells were detached and counted using a microcellcounter CC-110. ABNM-13 inhibited the growth of AsPC-1 cells with an IC₅₀ of 76 ± 4 μM.

3.2. Effect of ABNM-13 on the growth of HL-60 cells – alone and in combination with Ara-C

HL-60 cells were seeded at a concentration of 0.1×10^6 per ml and incubated with increasing concentrations of ABNM-13. After 24, 48, and 72 h, the cell number of viable leukemia cells was determined. ABNM-13 inhibited the growth of HL-60 cells with IC₅₀ values (IC₅₀ = 50% growth inhibition of tumor cells) of 15 ± 0.3 and 11 ± 1.1 μM, respectively (Fig. 2a). Exposure to ABNM-13 for 24 h resulted in a cell count of $67 \pm 0.6\%$ (33% growth inhibition). Treatment with HU, a RR inhibitor currently used in the clinic for 48 and 72 h resulted in IC₅₀ values of 143 ± 0.2 and 88 ± 0.2 μM, respectively (Fig. 2b). These findings are consistent with those obtained by Szekeres et al. who determined an IC₅₀ of 73 μM after 96 h of incubation [38].

To investigate the effect of ABNM-13 in combination with Ara-C, HL-60 cells were seeded at a concentration of 0.1×10^6 per ml and simultaneously or sequentially incubated with increasing

Table 1

Synergistic combination effects of ABNM-13 and Ara-C in HL-60 cells employing a sequential growth inhibition assay.

Compound	Concentration (μM/nM)	Cell number ± SD (% of control)	Predicted value ^a	Combination index ^b
ABNM-13 (A) (μM)	2.5	88.7 ± 0.78		
	5.0	61.8 ± 0.16		
	7.5	50.9 ± 0.78		
	10.0	32.6 ± 0.31		
Ara-C (B) (nM)	10	72.4 ± 0.94		
	15	71.8 ± 3.61		
	20	59.3 ± 3.45		
ABNM-13 + Ara-C	2.5			
	10	49.2 ± 4.55	64.2	0.607 ^c
ABNM-13 +Ara-C	2.5			
	15	25.2 ± 4.87	63.7	0.305 ^c
ABNM-13 +Ara-C	2.5			
	20	39.8 ± 2.35	52.6	0.607 ^c
ABNM-13 +Ara-C	5			
	10	15.5 ± 7.85	44.7	0.329 ^c
ABNM-13 +Ara-C	5			
	15	20.0 ± 5.65	44.4	0.418 ^c
ABNM-13 +Ara-C	5			
	20	32.1 ± 1.10	36.6	0.692 ^c
ABNM-13 +Ara-C	7.5			
	10	17.3 ± 5.02	36.9	0.514 ^c
ABNM-13 +Ara-C	7.5			
	15	26.4 ± 0.00	36.6	0.740 ^c
ABNM-13 +Ara-C	7.5			
	20	23.2 ± 1.41	30.2	0.695 ^c
ABNM-13 +Ara-C	10			
	10	17.2 ± 2.04	23.6	0.670 ^c
ABNM-13 +Ara-C	10			
	15	16.8 ± 1.73	23.4	0.676 ^c
ABNM-13 +Ara-C	10			
	20	17.9 ± 2.67	19.3	0.727 ^c

Cells were sequentially incubated with (1) ABNM-13 for 24 h and (2) Ara-C for 48 h, and then the cell number was determined. Data are means of two determinations ± standard deviations (SD).

^a Predicted value: (%A × %B)/100.

^b Combination indices according to the equation of Chou and Talalay [36].

^c Synergistic combination effect.

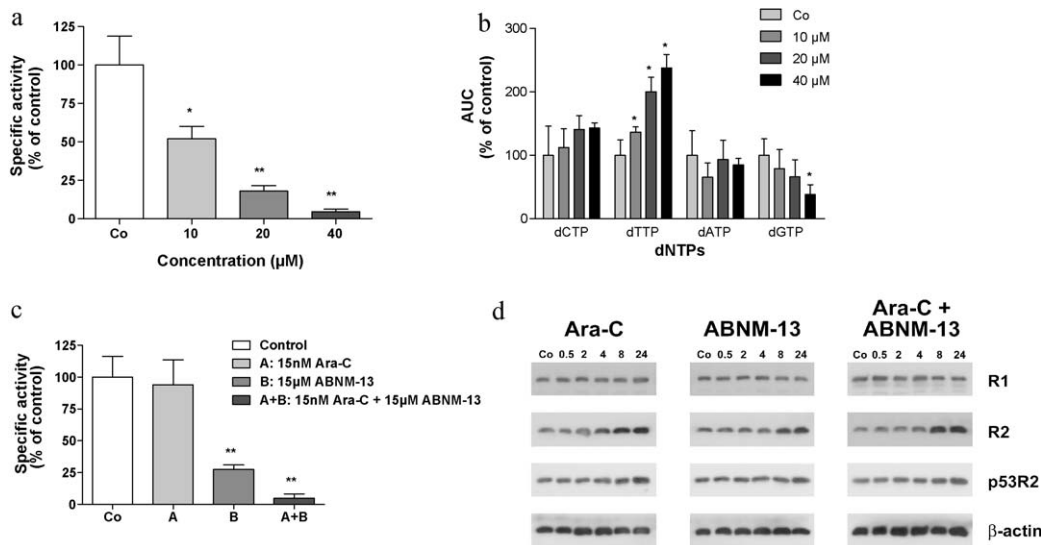


Fig. 3. (a) Inhibition of incorporation of ^{14}C -cytidine into DNA of HL-60 cells after treatment with ABNM-13 for 24 h (DNA synthesis assay). HL-60 cells (0.4×10^6 cells per ml) were incubated with increasing concentrations of ABNM-13 for 24 h. After the incubation period, cells were counted and pulsed with ^{14}C -cytidine (0.3125 μCi , 5 nM) for 30 min at 37 °C. Then cells were collected by centrifugation and washed with PBS. Total DNA was extracted from 5×10^6 cells and specific radioactivity of the samples was determined using a Wallac 1414 liquid scintillation counter (PerkinElmer, Boston, MA). Data are means \pm standard errors of three determinations. Values significantly ($p < 0.05$) different from control are marked with an asterisk (*). Highly significant ($p < 0.01$) differences are marked with two asterisks (**). (b) Concentration of dNTP pools in HL-60 cells upon treatment with ABNM-13. HL-60 cells (0.4×10^6 cells per ml) were incubated with 10, 20, and 40 μM ABNM-13 for 24 h. Afterwards, 5×10^7 cells were separated for the extraction of dNTPs. The concentration of dNTPs was calculated as percent of total area under the curve for each sample. Data are means \pm standard errors of three determinations. Values significantly ($p < 0.05$) different from control are marked with an asterisk (*). (c) Inhibition of incorporation of ^{14}C -cytidine into DNA of HL-60 cells after treatment with ABNM-13 and/or Ara-C for 30 min (DNA synthesis assay). HL-60 cells (0.4×10^6 cells per ml) were incubated with 15 μM ABNM-13 and/or 15 nM Ara-C and simultaneously pulsed with ^{14}C -cytidine (0.3125 μCi , 5 nM) for 30 min at 37 °C. Then cells were collected by centrifugation and washed with PBS. Total DNA was extracted from 5×10^6 cells and specific radioactivity of the samples was determined using a Wallac 1414 liquid scintillation counter (PerkinElmer, Boston, MA). Data are means \pm standard errors of three determinations. Highly significant ($p < 0.01$) differences are marked with two asterisks (**). (d) Expression levels of RR subunits R1, R2 and p53R2 in HL-60 cells upon treatment with ABNM-13 and/or Ara-C. After incubation with 15 μM ABNM-13 and/or 15 nM Ara-C for 0.5, 2, 4, 8, and 24 h, HL-60 cells (2×10^6 per ml) were harvested, washed twice with ice-cold PBS (pH 7.2) and lysed in a buffer containing 150 mM NaCl, 50 mM Tris-buffered saline (Tris pH 8.0), 1% Triton X-100, 1 mM phenylmethylsulfonylfluoride (PMSF) and protease inhibitor cocktail (PIC; from a 100 \times stock). The lysate was centrifuged at 12,000 rpm for 20 min at 4 °C, and the supernatant was subjected to Western blot analysis.

concentrations of drugs (ABNM-13 first for 24 h and then Ara-C for 48 h as described in the Section 2). All 12 drug combinations yielded additive effects when ABNM-13 and Ara-C were applied simultaneously (data not shown). Moreover, all 12 combinations led to highly synergistic effects when applied sequentially (cells were first incubated with 2.5, 5, 7.5, and 10 μM ABNM-13 followed by the addition of 5, 10, and 20 nM Ara-C, respectively) (Table 1).

3.3. Effect of ABNM-13 on the growth of AsPC-1 cell colonies

AsPC-1 cells were seeded at a concentration of 2×10^3 per well and incubated with increasing concentrations of ABNM-13. Colonies were counted after 6 days of treatment. ABNM-13 inhibited the growth of AsPC-1 cell colonies with an IC_{50} value of $11.5 \pm 1.4 \mu\text{M}$ (Fig. 2c) being almost identical to the IC_{50} seen in HL-60 cells ($11 \pm 1.1 \mu\text{M}$).

3.4. MTT chemosensitivity assay

AsPC-1 or HL-60 cells (5×10^3 per well) were seeded in 96-well microtiter plates and exposed to increasing concentrations of ABNM-13 as described in Section 2. After 96 h of incubation, ABNM-13 reduced the absorbance (viability) of AsPC-1 and HL-60 cells with IC_{50} values of 40 ± 3.4 and $9 \pm 1.7 \mu\text{M}$, respectively.

3.5. Inhibition of incorporation of ^{14}C -cytidine into DNA of HL-60 cells (DNA synthesis assay) and dNTP alterations after treatment with ABNM-13 and/or Ara-C

Incorporation of ^{14}C -cytidine into nascent DNA was measured in HL-60 cells after incubation with increasing concen-

trations of ABNM-13. Exposure to 10, 20, and 40 μM ABNM-13 for 24 h significantly decreased ^{14}C -cytidine incorporation to $52 \pm 13.9\%$, $17 \pm 6.1\%$, and $4 \pm 2.8\%$, respectively (Fig. 3a). Constitutive RR activity maintains balanced dNTP pools, whereas RR inhibition tilts this balance. In line with this, ABNM-13 treatment caused also an imbalance of dNTPs in HL-60 cells after 24 h, which was determined by HPLC analysis. Incubation of cells with 40 μM ABNM-13 resulted in a significant depletion of intracellular dGTP pools to $36 \pm 15.7\%$. Treatment with 10, 20, and 40 μM ABNM-13 significantly increased dTTP pools to $134 \pm 8.0\%$, $200 \pm 22.7\%$, and $237 \pm 21.3\%$ of control values, respectively. Regarding dCTP and dATP pools, treatment with ABNM-13 led to insignificant changes (Fig. 3b).

To analyze the immediacy of DNA synthesis inhibition, HL-60 cells were exposed to 15 nM Ara-C, 15 μM ABNM-13, and the simultaneous combination of both compounds for only 30 min. Even this short incubation period reduced the incorporation of ^{14}C -cytidine to $93 \pm 33.8\%$, $27 \pm 6.3\%$, and $4 \pm 5.7\%$ of controls, respectively (Fig. 3c).

3.6. Expression of RR subunits R1, R2, and p53R2 after treatment with ABNM-13 and/or Ara-C

To monitor the effect of RR inhibitors on the expression of RR subunits, HL-60 cells were incubated with 15 nM Ara-C and/or 15 μM ABNM-13 for 0.5, 2, 4, 8, and 24 h and subjected to Western blot analysis. The protein level of the constitutively expressed R1 subunit remained unchanged during the whole time course. R2 levels showed an increase after 8 and 24 h, and p53R2 levels were elevated after 24 h of incubation (Fig. 3d). Both R2 and p53R2 are S-phase specific.

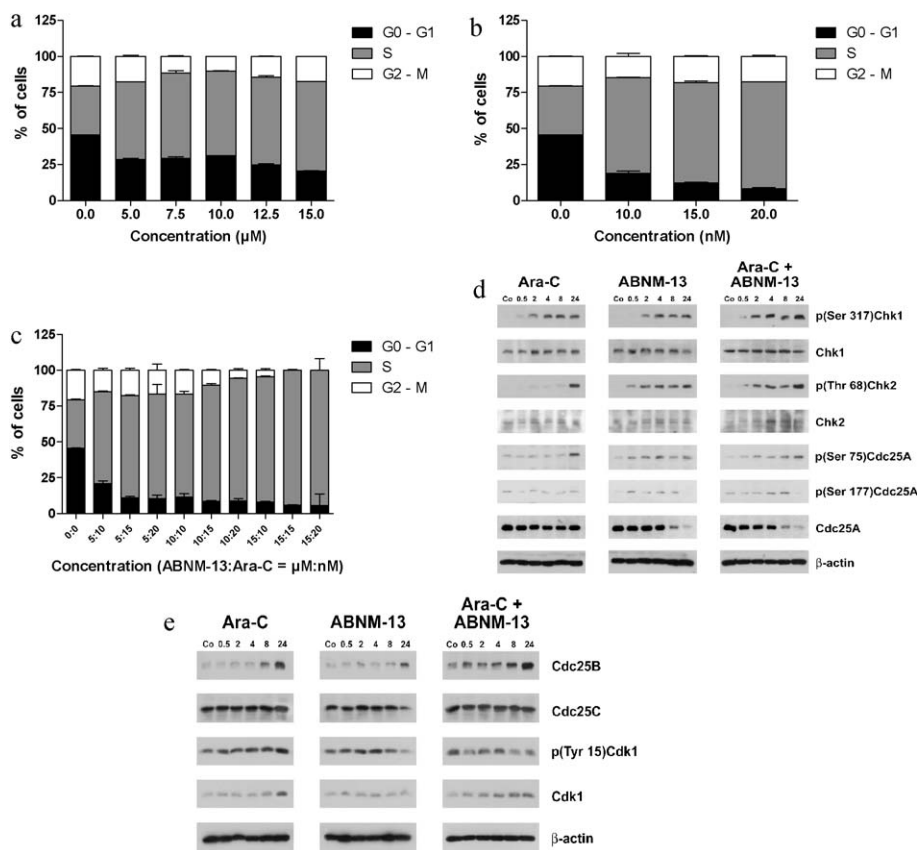


Fig. 4. (a–c) Cell cycle distribution in HL-60 cells after incubation with ABNM-13 and/or Ara-C. HL-60 cells (0.4×10^6 per ml) were seeded in 25 cm^2 Nunc tissue culture flasks and simultaneously incubated with 15 μM ABNM-13 and/or 15 nM Ara-C at 37 $^\circ\text{C}$ for 24 h under cell culture conditions. Cells were analyzed on a FACSCalibur flow cytometer (BD Biosciences, San Jose, CA, USA) and cell cycle distribution was calculated with ModFit LT software (Verity Software House, Topsham, ME, USA). Data are means \pm standard errors of three determinations. (d) Expression levels of p(Ser 317)Chk1, Chk1, p(Thr 68)Chk2, Chk2, p(Ser 75)Cdc25A, p(Ser 177)Cdc25A, and Cdc25A after incubation with ABNM-13 and/or Ara-C. After incubation with 15 μM ABNM-13 and/or 15 nM Ara-C for 0.5, 2, 4, 8, and 24 h, HL-60 cells (2×10^6 per ml) were harvested, washed twice with ice-cold PBS (pH 7.2) and lysed in a buffer containing 150 mM NaCl, 50 mM Tris-buffered saline (Tris pH 8.0), 1% Triton X-100, 1 mM phenylmethylsulfonylfluoride (PMSF) and protease inhibitor cocktail (PIC; from a 100 \times stock). The lysate was centrifuged at 12,000 rpm for 20 min at 4 $^\circ\text{C}$, and the supernatant was subjected to Western blot analysis. (e) Expression levels of Cdc25B, Cdc25C, p(Tyr 15)Cdk1, and Cdk1 after incubation with ABNM-13 and/or Ara-C. After incubation with 15 μM ABNM-13 and/or 15 nM Ara-C for 0.5, 2, 4, 8, and 24 h, HL-60 cells (2×10^6 per ml) were harvested, washed twice with ice-cold PBS (pH 7.2) and lysed in a buffer containing 150 mM NaCl, 50 mM Tris-buffered saline (Tris pH 8.0), 1% Triton X-100, 1 mM phenylmethylsulfonylfluoride (PMSF) and protease inhibitor cocktail (PIC; from a 100 \times stock). The lysate was centrifuged at 12,000 \times rpm for 20 min at 4 $^\circ\text{C}$, and the supernatant was subjected to Western blot analysis.

3.7. Cell cycle distribution in HL-60 cells after treatment with ABNM-13 and/or Ara-C

HL-60 cells were simultaneously incubated with 15 μM ABNM-13 and/or 15 nM Ara-C for 24 h. Treatment of HL-60 cells with 15 μM ABNM-13 caused cell cycle arrest in S-phase, increasing this cell population from $34 \pm 0.4\%$ to $62 \pm 0.0\%$, whereas G0–G1 phase cells decreased from $46 \pm 0.1\%$ to $21 \pm 0.1\%$. 15 nM Ara-C likewise caused an accumulation of $69 \pm 1.6\%$ HL-60 cells in S-phase and a concomitant decrease of G0–G1 cells to $12 \pm 0.8\%$. Simultaneous incubation of HL-60 cells with 15 μM ABNM-13 and 15 nM Ara-C led to an even more pronounced growth arrest in the S-phase, increasing this cell population from $34 \pm 0.4\%$ to $94 \pm 0.5\%$ while decreasing cells in the G0–G1 phase from $46 \pm 0.5\%$ to $6 \pm 0.5\%$ (Fig. 4a–c). No subG1 peaks could be observed by FACS at the time points measured.

3.8. Expression of checkpoint and cell cycle regulating proteins after treatment with ABNM-13 and/or Ara-C

To investigate whether S-phase inhibition caused activation of cell cycle checkpoint kinases, HL-60 cells were simultaneously treated with 15 nM Ara-C and/or 15 μM ABNM-13 for 0.5, 2, 4, 8, and 24 h and subjected to Western blot analysis (Fig. 4d and e). Chk1 was phosphorylated at the activating Ser317 site within

30 min (Ara-C), 2 h (ABNM-13), and 30 min (Ara-C/ABNM-13). Chk2 was phosphorylated at the activating Thr68 site within 24 h (Ara-C), 30 min (ABNM-13), and 30 min (ABNM-13/Ara-C). Chk1 protein levels remained unchanged, whereas Chk2 protein levels increased transiently, in particular when using the combination of ABNM-13 and Ara-C (Fig. 4d). In addition, ABNM-13 caused phosphorylation at Ser75 and Ser177 of the dual-specificity phosphatase Cdc25A, which are target sites of Chk1 and Chk2, respectively, resulting in its downregulation after 8 and 24 h. On the other hand, ABNM-13 upregulated Cdc25B protein levels after 24 h (Ara-C after 8 and 24 h), resulting in the dephosphorylation of Tyr15 of Cdk1 after 24 h, which is indicative for its activation (Fig. 4e). Ara-C treatment did not cause dephosphorylation of Cdk1. Cdc25C levels remained unchanged throughout the time course.

3.9. Induction of apoptosis in HL-60 cells by ABNM-13 and/or Ara-C

HL-60 cells were exposed to 12.5, 15, 17.5, and 20 μM ABNM-13 and/or 15 nM Ara-C for 24 and 48 h and double stained with Hoechst 33258 and propidium iodide to analyze whether apoptotic cell death was induced. The nuclear morphology of $16 \pm 0.9\%$ and $22 \pm 2.4\%$ HL-60 cells showed early or late apoptosis stages upon treatment with 15 μM ABNM-13 for 24 and 48 h, respectively (Fig. 5a). Incubation with 15 nM Ara-C or the combination of 15 μM

ABNM-13 and 15 nM Ara-C for 24 h resulted in only $8.2 \pm 0.5\%$ and $13 \pm 2.7\%$ apoptotic cells, respectively. Even the exposure of cells to 15 nM Ara-C or the combination of 15 μM ABNM-13 and 15 nM Ara-C for 48 h led to no more than $10 \pm 0.6\%$ and $28 \pm 4.8\%$ apoptotic cells, respectively, suggesting that cell death is at best additive but not synergistic after simultaneous application of both compounds (Fig. 5b). The induction of apoptosis was further substantiated by the cleavage and therefore activation of caspase-3 after 8 and 24 h of treatment with 15 μM ABNM-13 or the combination of 15 μM ABNM-13 and 15 nM Ara-C which in turn led to increased protein levels of γH2AX after 24 h (Fig. 5c). In contrast, 15 nM Ara-C induced activated caspase-3 and γH2AX levels only marginally. Constitutive phospho-ATM levels were not enhanced upon treatment with ABNM-13 and/or Ara-C. Examples of the cellular morphology are provided in Fig. 5d.

4. Discussion

3D molecular space modeling techniques were used to design *in silico* structures specifically to inhibit the activity of ribonucleotide reductase (RR), which is the rate-limiting enzyme of *de novo* DNA synthesis. From a panel of 13 compounds, we found that ABNM-13 is the most active agent with regard to growth inhibition of HL-60 cells.

The analysis of the *in situ* RR activity evidenced that ABNM-13 is a powerful RR inhibitor even after a short incubation time and at low concentrations. In addition, ABNM-13 caused alterations of deoxyribonucleoside triphosphate (dNTP) pool balance: dGTP pools were significantly depleted while dTTP pools were elevated. By misbalancing the concentration of precursors for *de novo* DNA synthesis, the latter is blocked in proliferating cells. Cell cycle

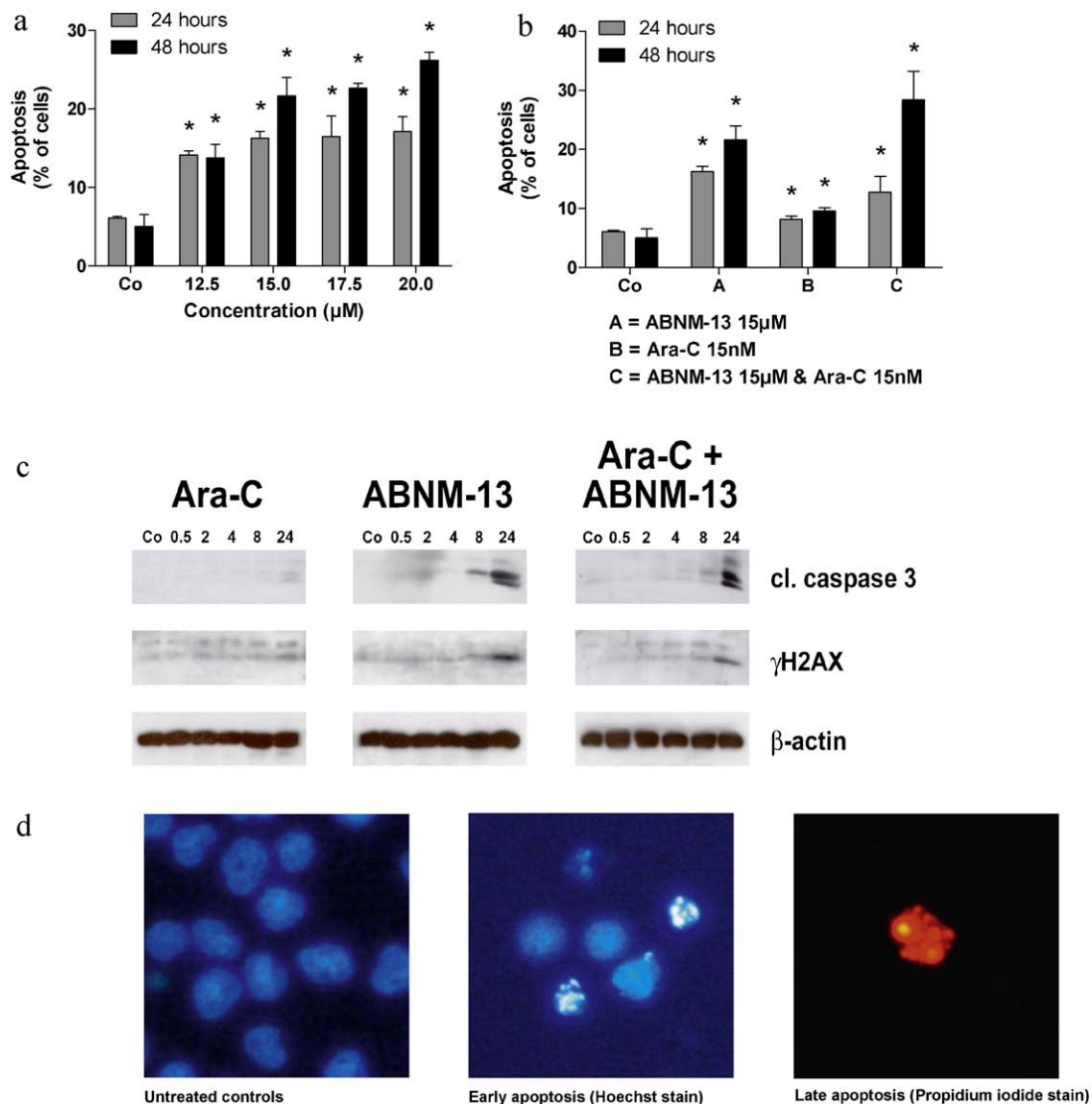


Fig. 5. (a and b) Induction of apoptosis in HL-60 cells after incubation with ABNM-13 and/or Ara-C. HL-60 cells (0.2×10^6 per ml) were exposed to increasing concentrations of ABNM-13 for 24 and 48 h (a) or treated with 15 μM ABNM-13 and/or 15 nM Ara-C for 24 and 48 h (b). Hoechst 33258 (HO, Sigma, St. Louis, MO, USA) and propidium iodide (PI, Sigma, St. Louis, MO, USA) were added directly to the cells to final concentrations of 5 $\mu\text{g}/\text{ml}$ and 2 $\mu\text{g}/\text{ml}$, respectively. After 60 min of incubation at 37 °C, cells were counted under a fluorescence microscope and the number of apoptotic cells was given as percentage value. Data are means \pm standard errors of three determinations. (c) Expression levels of cleaved caspase-3 and γH2AX after incubation with ABNM-13 and/or Ara-C. After incubation with 15 μM ABNM-13 and/or 15 nM Ara-C for 0.5, 2, 4, 8, and 24 h, HL-60 cells (2×10^5 per ml) were harvested, washed twice with ice-cold PBS (pH 7.2) and lysed in a buffer containing 150 mM NaCl, 50 mM Tris-buffered saline (Tris pH 8.0), 1% Triton X-100, 1 mM phenylmethylsulfonylfluoride (PMSF) and protease inhibitor cocktail (PIC; from a 100 \times stock). The lysate was centrifuged at 12,000 rpm for 20 min at 4 °C, and the supernatant was subjected to Western blot analysis. (d) Examples of the cellular morphology. After incubation with increasing concentrations of ABNM-13 for 48 h, HL-60 cells were double stained with Hoechst dye 33258 plus propidium iodide. In comparison to untreated controls, the cell morphology of HL-60 cells after treatment showed nuclear condensation and apoptotic bodies (early apoptosis) or loss of membrane integrity (late apoptosis).

perturbations, growth arrest and induction of apoptosis are the consequences, as it was observed in the course of ABNM-13 treatment.

The prime effect of ABNM-13 was a strong S-phase arrest which is consistent with the role of RR as the rate limiting enzyme for S-phase transit and the fact that inhibition of RR leads to inhibition of cells in S-phase [39]. It has been suggested that cells in which RR was inhibited by HU may enter the early S-phase at a normal rate and accumulate there until they undergo apoptosis [40,41]. The protein level of the constitutively expressed R1 subunit of RR remained unchanged. In contrast, the S-phase specific R2 subunit and also the p53R2 subunit of the enzyme were elevated although HL-60 cells are p53 deficient, indicating a compensatory up-regulation through which the cells try to rebalance their dNTP production. However, these findings are in line with the observations made by Yanomoto et al. [42] who demonstrated that basal levels of p53R2 are expressed regardless of the cellular p53 status and of Zhang et al. [43] who showed that up-regulation of the R2 protein levels occurs in response to DNA damage and involves up-regulation and activation of Chk1.

DNA damage or disrupted dNTP balance and incomplete DNA synthesis activate cell cycle checkpoints to prevent DNA synthesis and cell cycle progression [44–46] and to provide time for repair before the damage gets passed on to daughter cells or to allow for the reconstitution of the dNTP pools. These regulatory pathways govern the order and timing of cell cycle transitions to ensure completion of one cellular event prior to commencement of another. Before mitosis, cells have to pass G1–S, intra-S, and G2–M cell cycle checkpoints, which are controlled by their key regulators, ATR and ATM protein kinases, through activation of their downstream effector kinases Chk1 and Chk2, respectively [46,47]. Activated Chk1 and Chk2 phosphorylate the Cdc25A phosphatase at Ser75 and Ser177, respectively, and target it for proteasomal degradation. Cdc25A is an oncogene and required for cell cycle transit. Treatment with ABNM-13 activated both Chk1 and Chk2, the latter being phosphorylated within as little as 30 min.

Both Cdc25B and Cdc25C induce mitosis by activating Cdk1/cyclin B [48], and Cdc25B has been implicated as the initial phosphatase to activate Cdk1/cyclin B [49]. Activated Cdk1/cyclin B then phosphorylates and activates Cdc25C, which in turn keeps Cdk1/cyclin B active, creating a positive feedback loop that drives the cell through mitosis [50]. Cdc25B protein levels were upregulated by ABNM-13, leading to dephosphorylation and activation of Cdk1. Cdc25C levels remained unchanged. In contrast, Ara-C induced Cdk1 protein expression, and co-treatment with Ara-C and ABNM-13 resulted in both an increase of Cdk1 levels and subsequent increase of its activity. Undue overexpression of Cdc25B, i.e. when Cdc25A is unavailable, and consequent dephosphorylation of Cdk1/cyclin B, as observed in this study, was shown to induce cell cycle arrest by abrogating entry into mitosis [51]. Furthermore, Cdk2, as being regulated by Cdc25A, is required for S-phase progression [52]. Therefore, the combined effect of Cdc25A degradation and Cdc25B overexpression most likely caused the almost complete S-phase arrest induced by ABNM-13 alone and together with Ara-C (Fig. 6). Apoptosis upon treatment with ABNM-13 occurred in only 22% of cells (after 48 h), indicating that cell cycle inhibition rather than induction of programmed cell death seems to be the primary antineoplastic effect of ABNM-13. We therefore believe that a portion of treated cells was growing much slower than untreated controls, but did not undergo necrosis or apoptosis. The latter was further determined by the expression of cleaved caspase-3 (after 8 h) which in turn led to elevation of γ H2AX protein levels (after 24 h), suggesting that treatment with ABNM-13 was not the primary cause for DNA double strand breaks but the consequence of caspase-3 induced DNase activation. This was supported by the

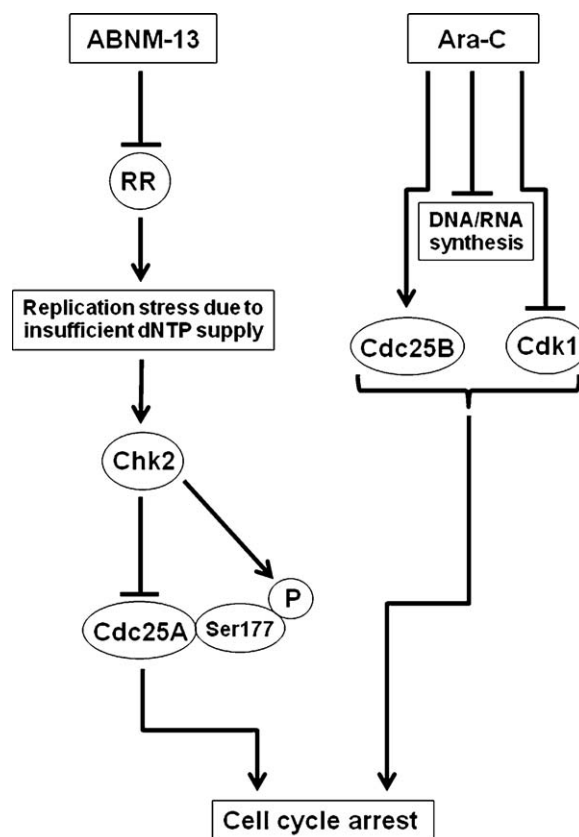


Fig. 6. Proposed mechanism of action of ABNM-13 and Ara-C.

fact that constitutive phospho-ATM levels were not elevated, either. Cell death via mitotic catastrophe (i.e. the formation of giant cells with two or more nuclei) being promoted by Chk2 inhibition [53,54] could not be observed at any time point.

Combination treatment is expected to produce fortified antitumor effects, if the pharmacokinetic and pharmacological properties are different from each other. Accordingly ABNM-13, which disregulated dTTP and dGTP pools and Ara-C, which is known to affect dCTP pools [55–57] inhibited cell proliferation synergistically. Using a sequential combination of ABNM-13 and Ara-C, all 12 concentrations applied yielded highly synergistic antineoplastic effects.

Taken together, we demonstrate that the novel RR inhibitor ABNM-13 exerts pronounced anticancer activity both as single agent and as enhancer of another antitumor drug such as Ara-C. Due to these promising results, ABNM-13 may support conventional chemotherapy of human malignancies and therefore deserves further preclinical and *in vivo* testing.

Acknowledgements

This investigation was supported by the “Fonds zur Foerderung der Wissenschaftlichen Forschung des Buergermeisters der Bundeshauptstadt Wien”, grant #09059 to M.F.-S., and the “Hochschuljubilaeumsstiftung der Stadt Wien”, grant #H-756/2005 to T.S. The authors wish to thank Toni Jaeger for preparing the Western blotting figures.

References

- [1] Koneru PB, Lien EJ, Avramis VI. Synthesis and testing of new antileukemic Schiff bases of N-hydroxy-N'-aminoguanidine against CCRF-CEM/0 human leukemia cells in vitro and synergism studies with cytarabine (Ara-C). *Pharmaceutical Research* 1993;10:515–20.

- [2] Ren S, Wang R, Komatsu K, Bonaz-Krause P, Zyrianov Y, McKenna CE, et al. Synthesis, biological evaluation, and quantitative structure–activity relationship analysis of new Schiff bases of hydroxysemicarbazide as potential antitumor agents. *Journal of Medicinal Chemistry* 2002;45:410–9.
- [3] Tai AW, Lien EJ, Lai MM, Khwaja TA. Novel N-hydroxyguanidine derivatives as anticancer and antiviral agents. *Journal of Medicinal Chemistry* 1984;27:236–8.
- [4] T'Ang A, Lien EJ, Lai MM. Optimization of the Schiff bases of N-hydroxy-N'-aminoguanidine as anticancer and antiviral agents. *Journal of Medicinal Chemistry* 1985;28:1103–6.
- [5] van't Riet B, Wampler GL, Elford HL. Synthesis of hydroxy- and amino-substituted benzohydroxamic acids: inhibition of ribonucleotide reductase and antitumor activity. *Journal of Medicinal Chemistry* 1979;22:589–92.
- [6] Matsumoto M, Fox JG, Wang PH, Koneru PB, Lien EJ, Cory JG. Inhibition of ribonucleotide reductase and growth of human colon carcinoma HT-29 cells and mouse leukemia L1210 cells by N-hydroxy-N'-aminoguanidine derivatives. *Biochemical Pharmacology* 1990;40:1779–83.
- [7] Takeda E, Weber G. Role of ribonucleotide reductase in expression in the neoplastic program. *Life Sciences* 1981;28:1007–14.
- [8] Kolberg M, Strand KR, Graff P, Andersson KK. Structure, function, and mechanism of ribonucleotide reductases. *Biochimica et Biophysica Acta* 2004;1699:1–34.
- [9] Shao J, Zhou B, Chu B, Yen Y. Ribonucleotide reductase inhibitors and future drug design. *Current Cancer Drug Targets* 2006;6:409–31.
- [10] Bourdon A, Minai L, Serre V, Jais JP, Sarzi E, Aubert S, et al. Mutation of RRM2B, encoding p53-controlled ribonucleotide reductase (p53R2), causes severe mitochondrial DNA depletion. *Nature Genetics* 2007;39:776–80.
- [11] Saban N, Bujak M. Hydroxyurea and hydroxamic acid derivatives as antitumor drugs. *Cancer Chemotherapy and Pharmacology* 2009;64:213–21.
- [12] Tennant L. Chronic myelogenous leukemia: an overview. *Clinical Journal of Oncology Nursing* 2001;5:218–9.
- [13] Noble S, Goa KL, Gemcitabine. A review of its pharmacology and clinical potential in non-small cell lung cancer and pancreatic cancer. *Drugs* 1997;54:447–72.
- [14] Toschi L, Finocchiaro G, Bartolini S, Gioia V, Cappuzzo F. Role of gemcitabine in cancer therapy. *Future Oncology* 2005;1:7–17.
- [15] Hatse S, De Clercq E, Balzarini J. Role of antimetabolites of purine and pyrimidine nucleotide metabolism in tumor cell differentiation. *Biochemical Pharmacology* 1999;58:539–55.
- [16] Abeysinghe RD, Greene BT, Haynes R, Willingham MC, Turner J, Planalp RP, et al. p53-independent apoptosis mediated by tachpyridine, an anti-cancer iron chelator. *Carcinogenesis* 2001;22:1607–14.
- [17] Samuni AM, Krishna MC, DeGraff W, Russo A, Planalp RP, Brechbiel MW, et al. Mechanisms underlying the cytotoxic effects of Tachpyr—a novel metal chelator. *Biochimica et Biophysica Acta* 2002;1571:211–8.
- [18] Turner J, Koumenis C, Kute TE, Planalp RP, Brechbiel MW, Beardsley D, et al. Tachpyridine, a metal chelator, induces G2 cell-cycle arrest, activates checkpoint kinases, and sensitizes cells to ionizing radiation. *Blood* 2005;106:3191–9.
- [19] Torti SV, Torti FM, Whitman SP, Brechbiel MW, Park G, Planalp RP. Tumor cell cytotoxicity of a novel metal chelator. *Blood* 1998;92:1384–9.
- [20] Greene BT, Thorburn J, Willingham MC, Thorburn A, Planalp RP, Brechbiel MW, et al. Activation of caspase pathways during iron chelator-mediated apoptosis. *Journal Biological Chemistry* 2002;277:25568–75.
- [21] Tsimberidou AM, Alvarado Y, Giles FJ. Evolving role of ribonucleoside reductase inhibitors in hematologic malignancies. *Expert Review of Anticancer Therapy* 2002;2:437–48.
- [22] Erlichman C, Fine S, Wong A, Elhakim T. A randomized trial of fluorouracil and folinic acid in patients with metastatic colorectal carcinoma. *Journal of Clinical Oncology* 1988;6:469–75.
- [23] Saiko P, Ozsvar-Kozma M, Bernhaus A, Jaschke M, Graser G, Lackner A, et al. N-hydroxy-N'-(3,4,5-trimethoxyphenyl)-3,4,5-trimethoxy-benzamidine, a novel resveratrol analog, inhibits ribonucleotide reductase in HL-60 human promyelocytic leukemia cells: synergistic antitumor activity with arabinofuranosylcytosine. *International Journal of Oncology* 2007;31:1261–6.
- [24] Horvath Z, Saiko P, Illmer C, Madlener S, Hoecht T, Bauer W, et al. Synergistic action of resveratrol, an ingredient of wine, with Ara-C and tiazofurin in HL-60 human promyelocytic leukemia cells. *Experimental Hematology* 2005;33:329–35.
- [25] Horvath Z, Murias M, Saiko P, Erker T, Handler N, Madlener S, et al. Cytotoxic and biochemical effects of 3,3',4,4',5,5'-hexahydroxystilbene, a novel resveratrol analog in HL-60 human promyelocytic leukemia cells. *Experimental Hematology* 2006;34:1377–84.
- [26] Fritzer-Szekeres M, Salamon A, Grusch M, Horvath Z, Hoecht T, Steinbrugger R, et al. Trimidox, an inhibitor of ribonucleotide reductase, synergistically enhances the inhibition of colony formation by Ara-C in HL-60 human promyelocytic leukemia cells. *Biochemical Pharmacology* 2002;64:481–5.
- [27] Fritzer-Szekeres M, Savinc I, Horvath Z, Saiko P, Penzberger M, Graser G, et al. Biochemical effects of piceatannol in human HL-60 promyelocytic leukemia cells—synergism with Ara-C. *International Journal of Oncology* 2008;33:887–92.
- [28] Szekeres T, Gharehbaghi K, Fritzer M, Woody M, Srivastava A, van't Riet B, et al. Biochemical and antitumor activity of trimidox, a new inhibitor of ribonucleotide reductase. *Cancer Chemotherapy and Pharmacology* 1994;34:63–6.
- [29] Garrett C, Santi DV. A rapid and sensitive high pressure liquid chromatography assay for deoxyribonucleoside triphosphates in cell extracts. *Analytical Biochemistry* 1979;99:268–73.
- [30] Grusch M, Polgar D, Gfatter S, Leuhuber K, Huettenbrenner S, Leisser C, et al. Maintenance of ATP favours apoptosis over necrosis triggered by benzamide riboside. *Cell Death and Differentiation* 2002;9:169–78.
- [31] Grasl-Kraupp B, Ruttkay-Nedecky B, Koudelka H, Bukowska K, Bursch W, Schulte-Hermann R. In situ detection of fragmented DNA (TUNEL assay) fails to discriminate among apoptosis, necrosis, and autolytic cell death: a cautionary note. *Hepatology* 1995;21:1465–8.
- [32] Rosenberger G, Fuhrmann G, Grusch M, Fassl S, Elford HL, Smid K, et al. The ribonucleotide reductase inhibitor trimidox induces c-myc and apoptosis of human ovarian carcinoma cells. *Life Sciences* 2000;67:3131–42.
- [33] Grusch M, Fritzer-Szekeres M, Fuhrmann G, Rosenberger G, Luxbacher C, Elford HL, et al. Activation of caspases and induction of apoptosis by novel ribonucleotide reductase inhibitors amidox and didox. *Experimental Hematology* 2001;29:623–32.
- [34] Fritzer-Szekeres M, Grusch M, Luxbacher C, Horvath S, Krupitza G, Elford HL, et al. Trimidox, an inhibitor of ribonucleotide reductase, induces apoptosis and activates caspases in HL-60 promyelocytic leukemia cells. *Experimental Hematology* 2000;28:924–30.
- [35] Huettenbrenner S, Maier S, Leisser C, Polgar D, Strasser S, Grusch M, et al. The evolution of cell death programs as prerequisites of multicellularity. *Mutation Research* 2003;543:235–49.
- [36] Chou TC, Talalay P. Quantitative analysis of dose–effect relationships: the combined effects of multiple drugs or enzyme inhibitors. *Advances in Enzyme Regulation* 1984;22:27–55.
- [37] Chou TC, Talalay P. Generalized equations for the analysis of inhibitions of Michaelis–Menten and higher-order kinetic systems with two or more mutually exclusive and nonexclusive inhibitors. *European Journal of Biochemistry (FEBS)* 1981;115:207–16.
- [38] Szekeres T, Fritzer M, Strobl H, Gharehbaghi K, Findenig G, Elford HL, et al. Synergistic growth inhibitory and differentiating effects of trimidox and tiazofurin in human promyelocytic leukemia HL-60 cells. *Blood* 1994;84:4316–4321.
- [39] Chimpoy K, Diaz GD, Li Q, Carter O, Dashwood WM, Mathews CK, et al. E2F4 and ribonucleotide reductase mediate S-phase arrest in colon cancer cells treated with chlorophyllin. *International Journal of Cancer* 2009;125:2086–94.
- [40] Yarbrow JW. Mechanism of action of hydroxyurea. *Seminars in Oncology* 1992;19:1–10.
- [41] Maurer-Schultze B, Siebert M, Bassukas ID. An in vivo study on the synchronizing effect of hydroxyurea. *Experimental Cell Research* 1988;174:230–43.
- [42] Yanamoto S, Iwamoto T, Kawasaki G, Yoshitomi I, Baba N, Mizuno A. Silencing of the p53R2 gene by RNA interference inhibits growth and enhances 5-fluorouracil sensitivity of oral cancer cells. *Cancer Letters* 2005;223:67–76.
- [43] Zhang YW, Jones TL, Martin SE, Caplen NJ, Pommier Y. Implication of checkpoint kinase-dependent up-regulation of ribonucleotide reductase R2 in DNA damage response. *Journal of Biological Chemistry* 2009;284:18085–9.
- [44] Kastan MB, Bartek J. Cell-cycle checkpoints and cancer. *Nature* 2004;432:316–23.
- [45] Shiloh Y. ATM and related protein kinases: safeguarding genome integrity. *Nature Reviews Cancer* 2003;3:155–68.
- [46] Bartek J, Lukas J, Chk1 and Chk2 kinases in checkpoint control and cancer. *Cancer Cell* 2003;3:421–9.
- [47] Abraham RT. Cell cycle checkpoint signaling through the ATM and ATR kinases. *Genes Development* 2001;15:2177–96.
- [48] Donzelli M, Draetta GF. Regulating mammalian checkpoints through Cdc25 inactivation. *EMBO Reports* 2003;4:671–7.
- [49] Nishijima H, Nishitani H, Seki T, Nishimoto T. A dual-specificity phosphatase Cdc25B is an unstable protein and triggers p34(cdc2)/cyclin B activation in hamster BHK21 cells arrested with hydroxyurea. *Journal of Cell Biology* 1997;138:1105–16.
- [50] Hoffmann I, Clarke PR, Marcote MJ, Karsenti E, Draetta G. Phosphorylation and activation of human cdc25-C by cdc2–cyclin B and its involvement in the self-amplification of MPF at mitosis. *EMBO Journal* 1993;12:53–63.
- [51] Varmeh-Ziaie S, Manfredi JJ. The dual specificity phosphatase Cdc25B, but not the closely related Cdc25C, is capable of inhibiting cellular proliferation in a manner dependent upon its catalytic activity. *Journal of Biological Chemistry* 2007;282:24633–41.
- [52] Donzelli M, Squatrito M, Ganoth D, Hershko A, Pagano M, Draetta GF. Dual mode of degradation of Cdc25 A phosphatase. *EMBO Journal* 2002;21:4875–84.
- [53] Castedo M, Perfettini JL, Roumier T, Andreau K, Medema R, Kroemer G. Cell death by mitotic catastrophe: a molecular definition. *Oncogene* 2004;23:2825–2837.
- [54] Portugal J, Mansilla S, Bataller M. Mechanisms of drug-induced mitotic catastrophe in cancer cells. *Current Pharmaceutical Design* 2010;16:69–78.
- [55] Gandhi V, Huang P, Chapman AJ, Chen F, Plunkett W. Incorporation of fludarabine and 1-beta-D-arabinofuranosylcytosine 5'-triphosphates by DNA polymerase alpha: affinity, interaction, and consequences. *Clinical Cancer Research* 1997;3:1347–55.
- [56] Wills PW, Hickey R, Malkas L. Ara-C differentially affects multiprotein forms of human cell DNA polymerase. *Cancer Chemotherapy and Pharmacology* 2000;46:193–203.
- [57] Seymour JF, Huang P, Plunkett W, Gandhi V. Influence of fludarabine on pharmacokinetics and pharmacodynamics of cytarabine: implications for a continuous infusion schedule. *Clinical Cancer Research* 1996;2:653–8.